Check for updates

Broadly tunable linewidth-invariant Raman Stokes comb for selective resonance photoionization

Daniel T. Echarri,[1,2] ⓘ Katerina Chrysalidis,[1] ⓘ Valentin N. Fedosseev,[1] Bruce A. Marsh,[1] Richard P. Mildren,[3] ⓘ Santiago M. Olaizola,[2,4] David J. Spence,[3] ⓘ Shane G. Wilkins,[1] and Eduardo Granados[1,*]

[1] *CERN, 1217 Geneva, Switzerland*
[2] *Universidad de Navarra, Tecnun, Manuel Lardizabal 13, 20018 Donostia / San Sebastián, Spain*
[3] *MQ Photonics Research Centre, Macquarie University, 2109 Sydney, Australia*
[4] *Ceit, Manuel Lardizabal 15, 20018 Donostia / San Sebastián, Spain*
[*] *eduardo.granados@cern.ch*

Abstract: We demonstrate a continuously tunable, multi-Stokes Raman laser operating in the visible range (420 - 600 nm). Full spectral coverage was achieved by efficiently cascading the Raman shifted output of a tunable, frequency-doubled Ti:Sapphire laser. Using an optimized hemi-spherical external Raman cavity composed only of a diamond crystal and a single reflecting mirror, producing high power output at high conversion efficiency ($>60\%$ from pump to Stokes) for a broad range of wavelengths across the visible. Enhancement of the cascading was achieved by controlling the polarization state of the pump and Stokes orders. The Stokes outputs exhibited a linewidth of 11 ± 1 GHz for each order, resembling the pump laser linewidth, enabling its use for the intended spectroscopic applications. Furthermore, the Raman laser performance was demonstrated by applying it for the resonance excitation of atomic transitions in calcium.

1. Introduction

Tunable lasers enable the study of electronic structure in atoms and molecules with high precision [1], granted that the parameters of excitation of light are matched to the quantum transitions in the species under study. In most cases, this implies that it is highly desirable to utilize lasers with emission linewidth matched to the experimental conditions, while maintaining the required wavelength tunability and peak power [2]. For the particular application of resonance ionization spectroscopy (RIS) [3], optimal efficiency requires that the laser linewidth is matched to the Doppler-broadened atomic lines, including fine and hyperfine structure splittings, which can typically be in the range of 5-15 GHz. Due to its high sensitivity, the method of laser resonance ionization is broadly used in studies of rare and radioactive atoms [4]. In particular, at ISOLDE/CERN and other on-line isotope separation facilities, radioactive ion beams are produced using the Resonance Ionization Laser Ion Source (RILIS) technique [5].

The energy range of strong electronic transitions in atoms corresponds to a broad spectral range from the UV to the IR. In the RILIS setup at ISOLDE/CERN, wide spectral coverage is achieved by combining dye lasers with Ti:Sapphire lasers [5–7]. Complemented by harmonic generation, the RILIS laser system is capable to cover the spectral range of 210-950 nm. However, tunable light in the visible range is generated by dye lasers, which require more maintenance (due to laser-dye degradation) in comparison to fully solid-state laser systems. Dye laser maintenance when producing wavelengths < 540 nm, which requires UV pumping, is particularly challenging. The Raman effect in crystalline media offers a convenient and reliable all-solid-state alternative to the dye laser, bridging the 450-650 nm range that is not easily covered by Ti:Sapphire laser

[8]. This solution avoids the need of frequent dye exchanges and therefore enables continuous long-term operation. Stimulated Raman Scattering (SRS) has already shown great potential for this purpose: the efficiency levels surpassed other non-linear optical techniques such as wave mixing or frequency doubling [9], and when a resonator is used they cleanup the pump laser profile producing high quality and brightness beams [10].

Recently, a Raman resonator was proposed for RIS applications [11], producing tunable, linewidth-invariant, 1st Stokes output with a power conversion efficiency of 28%. This initial study was limited to the generation of only the first Stokes order. While its output was already useful for some spectroscopic experiments, its wavelength coverage was essentially limited to a single Raman shift in diamond ($\Delta\omega_R = 1332$ cm^{-1}). Cascading the Raman process has the potential to extend the wavelength coverage considerably at no cost maintaining its high-intensity operation [12]. There are multiple demonstrations of efficient cascaded Raman lasers, however, the magnitude and behaviour of the Stokes linewidth through the cascading process has yet to be studied in detail [9,12,13]. In this work, we performed linewidth measurements of the cascaded orders in order to identify the conditions required for generating higher-order Stokes emission with nearly identical spectral properties.

Fully continuous tunability using cascaded Raman conversion is reached when the tuning range of the pump laser is larger than the Raman shift ($\Delta\omega_P > \Delta\omega_R$). To the best of our knowledge, the present work represents the first demonstration of such performance across the visible spectral range. In general, most Raman crystalline materials produce a shift between 770 - 1085 cm^{-1} [9], which at a pump wavelength of 400 nm set a minimum tunability requirement of $\sim$ 16 - 23 nm. Consequently the second harmonic of a Ti:Sapphire laser is a natural candidate for producing multiple Stokes orders covering the entire visible spectral range.The choice of Raman media depends upon multiple factors, including $\Delta\omega_P$, the Raman gain, and the spectral range to be covered. Of the Raman active crystalline materials suitable for lasing between 420 - 600 nm, diamond is the most suitable for operating at high power [14,15] and provides a large Raman shift combined with high Raman gain [16,17]. The wide spectral transparency of diamond enables its use for producing light from the deep-UV [18] to the mid-IR [19], it has been integrated on a chip [20], and monolithic versions have been realized [21]. Currently, single longitudinal mode (SLM) diamond Raman lasers are being employed in applications such as gas detection experiments [22]. The study of spectral effects in Raman lasers is a growing area of research, although spectral effects in cascaded Raman processes remain poorly understood [23].

In this paper, we present a flexible, compact and efficient cascaded Raman laser covering the entire visible spectral range (420 - 600 nm) using an optimized resonator design. The experimental results are accompanied by the theoretical description of the dependency of the cascading efficiency on polarization, and the conditions to maintain the pump laser linewidth for higher Stokes orders. Furthermore, we show the first demonstration of GHz-resolution spectroscopy utilizing a Raman laser.

2. Fully tunable cascaded Raman laser

A schematic diagram of the experimental setup is shown in Fig. 1. The pump light at 450 nm was provided by an intra-cavity frequency-doubled Ti:Sapphire laser with a Z-cavity layout (for further details see [7]). Frequency selection was obtained by the combination of an intra-cavity birefringent filter and a thin (0.3 mm) Fabry-Perot etalon, while frequency conversion was achieved using a 6 mm long BiB$_3$O$_6$ (BiBO) crystal. The tunability range covered wavelengths from 350 - 450 nm. The system produced approximately 1.2 W of average power at 10 kHz repetition rate with a pulse duration of 50 ns. A broadband zero order half-wave-plate (HWP) was placed in the pump beamline to enable polarisation rotation. The output was focused into the diamond crystal using a +150 mm focal length lens, producing a waist of 60 ± 5 μm in diameter. The linewidth (FWHM) of the Ti:Sapphire output was measured with a wavelength

meter (LM-007 *(CLUSTER LTD Moscow)*), and was found to be 10.4 ± 0.2 GHz. This linewidth is about a factor of $\sqrt{2}$ wider than the fundamental linewidth of the Ti:Sapphire laser at 800 nm.
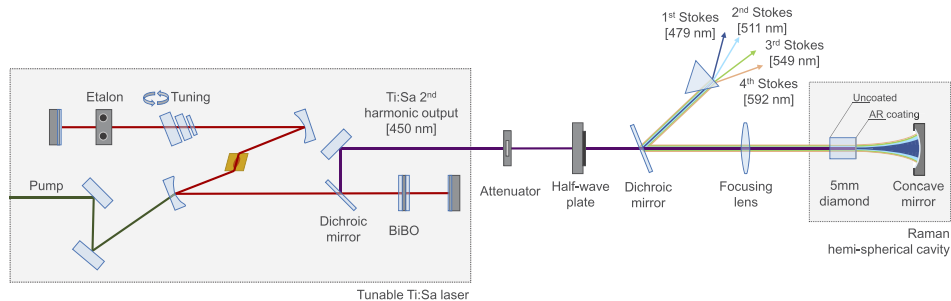
Fig. 1. Schematic layout of the Raman laser set up: An intra-cavity frequency-doubled Ti:Sapphire laser at 450 nm was used for pumping a diamond crystal. The cavity (dotted box) consists of a hemi-spherical resonator. The output coupler of the Raman cavity is the uncoated diamond surface at the pump-input side. Optical elements are not shown to scale.

The Raman medium is a synthetic single-crystal diamond (low-birefringence, low-nitrogen, CVD-grown single crystal, from *Element Six Ltd.*) with dimensions of 5 mm (length) x 5 mm (width) x 1 mm (height) and plane-cut for beam propagation along the <110> axis. In order to minimize potential spectral effects introduced by the diamond crystal faces [24], one of them was covered with a broadband (450 - 650 nm) anti-reflective coating. The laser cavity was therefore encompassed by the uncoated diamond surface (the output coupler) and the broadband-reflective concave spherical mirror (ROC = 50 mm) , as depicted in Fig. 1. The output coupling was 85%, which was optimal for the used pumping configuration within the available standard optics (~100 μJ, 60 μm diameter spot).

The resonator shown here is substantially different from the previously reported extra-cavity nanosecond diamond Raman lasers [11,25–27]. In our case, the low pulse energy (in the ~100 μJ level) necessitates a small beam waist in the resonator cavity, conducive to the use of short focal length concave mirrors. This led to an effective resonator length as short as 5 cm, improving the Raman conversion efficiency. The output of the Raman cavity was collinear and counter-propagating with respect to the pump beam, and so a flat short-pass dichroic mirror with a cutoff wavelength of 420 nm was used for separating the Stokes outputs from the pump. To enable broadband operation, the angle of this dichroic mirror was adjusted to obtain an optimal combination of pump transmission and Stokes orders reflection. The Stokes output orders were then separated by a dispersive prism.

The diamond crystal tip-tilt angles and distance with respect to the curved mirror were adjusted in order to maximize the cascaded Stokes output power, obtaining a well-matched cavity waist of ~60 μm in diameter ($1/e^2$). The optimal distance between the input diamond surface and the mirror was found to be approximately 48 mm. The total round-trip time of the cavity was estimated to be 0.37 ns, which is 2 orders of magnitude less than the pump pulse duration of 50 ns, enabling highly efficient Raman conversion.

2.1. Higher-order Stokes gain and polarization

The generation of the second and higher-order Stokes can be seeded by a parametric four-wave mixing (FWM) process. The contribution of the parametric coupling to SRS power is however dependant on the fulfillment of the phase matching condition for partly degenerate FWM:

$$2\mathbf{k}_j = \mathbf{k}_{j-1} + \mathbf{k}_{j+1} \tag{1}$$

where j is the number of the SRS component ($j<0$ for an anti-Stokes wave, $j>0$ for a Stokes wave, and $j = 0$ for the SRS pump wave). $\mathbf{k}_j$ is the wave vector of the FWM pump, and $\mathbf{k}_{j-1}$ and $\mathbf{k}_{j+1}$ are the wave vectors of the neighbouring SRS components, which are the signal and idler waves of the FWM process. For collinear geometry a phase mismatch is produced, and can be calculated from the equation:

$$\Delta k_j = k_{j-1} + k_{j+1} - 2k_j. \tag{2}$$

Here k_j, k_{j-1} and k_{j+1} are the moduli of the corresponding wave vectors. Generally, this expression violates the condition (1). The principal cause for the phase mismatch is the dispersion due to the refractive index of the medium, which weakens the efficiency of the parametric coupling [28]. In this paper, we therefore assumed that the FWM contribution for Stokes generation was negligible.

We now then derive equations for non FWM-seeded conditions. This approximation is equivalent to assuming that the nth Stokes wave experiences SRS gain pumped exclusively by the $(n-1)^{\text{th}}$ Stokes field, with gain and polarization depending only on the $(n-1)^{\text{th}}$ Stokes order polarization and intensity.

In general, the Raman scattering tensors describe the direction and magnitude of the induced polarization in the Stokes orders as a function of pump polarization angle. The net effect of the Raman scattering tensors can be formulated as a Müller matrix that allows a direct calculation of the polarization effects in the Raman scattering process [29]. For propagation along the <110> axis, the Stokes polarization and the Raman gain coefficient depends on the polarization of the pump laser by $\mathbf{S} = \mathbf{M}_{<110>}\mathbf{P}$, where the vectors $\mathbf{S}$ and $\mathbf{P}$ are the polarization states of Stokes and pump waves respectively represented in the Poincaré sphere. $\mathbf{M}_{<110>}$ is the Müller matrix for the propagation direction along <110>.

Typically the vibrational modes can either be A, E or F in a diamond lattice. In our experiments, we concluded that the F modes were excited preferentially by performing polarization measurements. While the 1$^{\text{st}}$ Stokes polarization rotated 90° with respect to the pump polarization angle (for $\psi_{<100>} = 0°$), the higher Stokes orders tended to be polarized in the vicinity of the 54.7° angle (i. e. aligned with the <111> axis).

For such excitation arrangement, it can be shown that the Stokes gain is proportional to: $g_S \propto I_P + I_U/2$, where $I_P = \sqrt{S_2^2 + S_3^2 + S_4^2}$ and $I_U = S_1 - I_P$. Analytically, this corresponds to an ith Stokes polarization angle given by:

$$\theta_i = \frac{\pi}{2} - \frac{1}{2}\left[\arctan\left(\frac{2sin(2\theta_{i-1})}{1 + cos(2\theta_{i-1})}\right)\right] \tag{3}$$

where θ_{i-1} is the polarization angle of the lower Stokes order, and $\theta_0 = \psi_{<100>}$ is the pump polarization angle. Analogously, it is possible to obtain analytical expressions for each Stokes order's gain g_{Si} scaling as a function of lower order polarization angle (θ_{i-1}):

$$= g_{Si} \propto 3 - cos(2\theta_{i-1}) + \sqrt{2 + 2cos(2\theta_{i-1}) + 3sin^2(2\theta_{i-1})} \tag{4}$$

Figure 2 shows the gain and polarization of three cascaded orders as a function of the pump polarization angle with respect to the <100> axis. As can be seen, for input polarization along the <111> axis, all Stokes orders have the same polarization and the highest gain [25]. This is the most efficient approach to cascading.

In order to inhibit the cascading, it is possible to simply align the pump polarization angle parallel to the axis <100>. The first Stokes would then have a perpendicular polarization with respect to the pump, while the gain for higher cascaded orders would be suppressed. The polarization angle of all higher Stokes orders converge to the <111> axis angle (54.7°). Consequently, it is not possible to use polarization-tuning to optimize the cascading into a specific higher Stokes order.
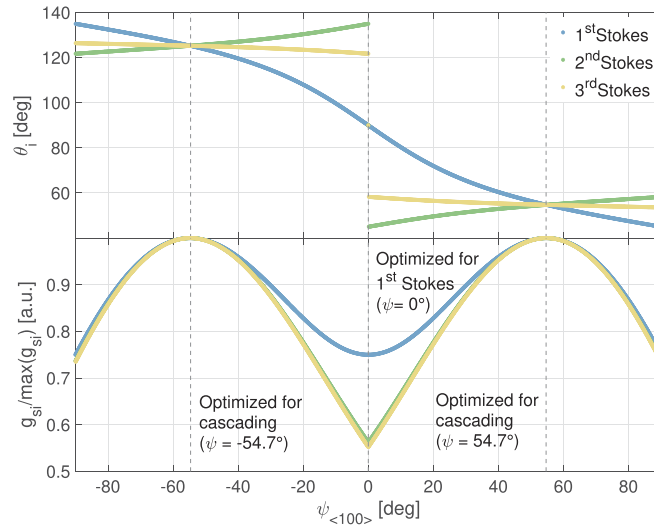
Fig. 2. (top) Polarization angle of ith Stokes order as a function of pump polarization angle with respect to the <100> crystallographic axis. (bottom) Relative Raman gain of ith Stokes order as a function of pump polarization angle with respect to the <100> crystallographic axis.

### 2.2. Measurements of the conversion efficiency for optimal pump polarization states

When optimized for 1st Stokes generation, the slope efficiency was measured to be 93 %, with an absolute efficiency of 42 % at maximum pump power as it can be seen in Fig. 3 and Table 1. The measurements for the 2nd Stokes were performed with polarization parallel to the <111> axis, and yielded a slope efficiency of 57 %. The 3rd Stokes lasing threshold did not allow accurate calculation of its slope efficiency. These results where obtained by optimizing the average power of each Stokes order. As shown in Fig. 3, the values at which the 2nd and 3rd Stokes are maximized, correspond to $54° \pm 1°$ and $52° \pm 1°$ respectively. This confirms the theoretical result obtained earlier, where the angle of maximum cascading to higher Stokes orders was shown to be $54.7°$.

Table 1. Summary of cascading performance for various input parameters at a pump power of 932 mW

	$\psi_{<100>}$	θ_i	Power	Conversion eff.
1st Stokes	$0° \pm 1°$	$90° \pm 1°$	400 mW	42%
2nd Stokes	$0° \pm 1°$	$50° \pm 1°$	139 mW	15%
3rd Stokes	$0° \pm 1°$	-	-	0%
1st Stokes	$54° \pm 1°$	$54° \pm 1°$	322 mW	35%
2nd Stokes	$54° \pm 1°$	$54° \pm 1°$	180 mW	19%
3rd Stokes	$52° \pm 1°$	$54° \pm 1°$	40 mW	3%

To provide further evidence of the near quantum limited operation, we also measured the residual pump power and the output Stokes power simultaneously as well as their temporal profiles, for a pump polarization angle of $\psi_{<100>} = 0°$ (shown in Fig. 4). The losses due to each optical element were calibrated with the un-depleted pump pulse in order to minimize experimental errors. For a maximum pump power of 932 mW, approximately 400 mW of 1st Stokes output was produced (power conversion efficiency of 42 %). The pump pulse temporal
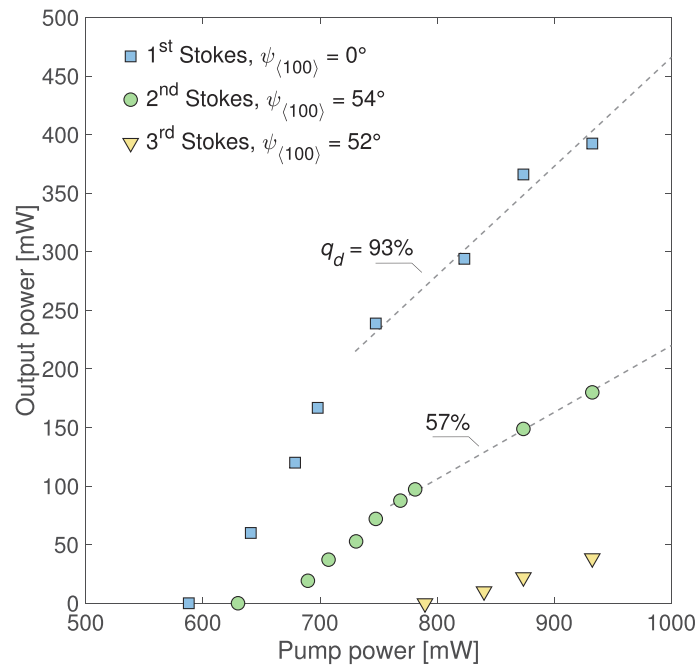
Fig. 3. Measured output power and slope efficiencies for the first three Stokes orders. q_d is the theoretical slope efficiency for the 1st Stokes taking into account solely the quantum defect. The pump polarization angle was adjusted to optimize output power at each Stokes order. When optimizing between the 2nd and 3rd Stokes orders, the improvement in power from tuning the pump polarization angle was small.

profile exhibited a sharp leading edge and a slowly decaying tail that does not contribute to Raman conversion, and results from the design of the gain-switched Ti:Sapphire resonator optical elements. Consequently, the Raman lasing threshold was quickly reached, producing in turn pulses with a steep leading edge resembling that of the pump pulse.

In terms of the peak power conversion efficiency, the pump laser peaked at 2.7 kW, whereas the 1st Stokes was 1.1 kW (40 % peak power conversion efficiency) with a pulse duration of 35 ns. We again calculated the slope efficiency from the synchronized temporal profiles with a bining larger than the cavity photon lifetime. Note that this method does not take into account the contribution of the pump pulse trailing edge that falls below lasing threshold. This measurement yielded a slope efficiency of approximately 92 ± 2 %, which validates the measurements performed for the Stokes power and slope efficiencies given in Fig. 3. The fact that the measured slope efficiency is marginally lower than the quantum efficiency is possibly owing to minor parasitic losses at the pump and Stokes wavelengths. Analogously, the 2nd Stokes presented a 15 % conversion efficiency, while its peak power conversion efficiency was approximately 27 %, with a pulse duration of 20 ns (54 round-trips). Once the second Stokes threshold was reached, partial conversion of first Stokes to 511 nm hinders subsequent conversion of the pump to the first Stokes. This is observed by a small positive slope in the residual pump signal.

The output beam quality was measured using a beam profiler (*Coherent Inc. LaserCam-HR II*) for all Stokes orders when the cavity was optimized for cascading. All orders exhibited a beam quality of the order of $M^2 < 1.3$, and slightly smaller than the one measured for the Ti:Sapphire pump laser, beam profiles are illustrated in Fig. 5. A table summarizing the cascaded performance for various pump polarization angles is given in Table 1.
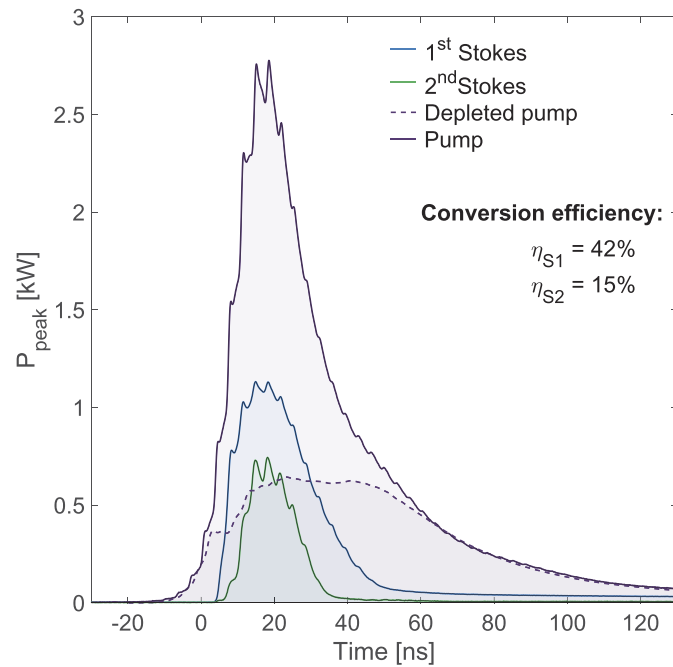
Fig. 4. Averaged pump, residual pump and Stokes pulses for pump polarization aligned with the <100> axis.
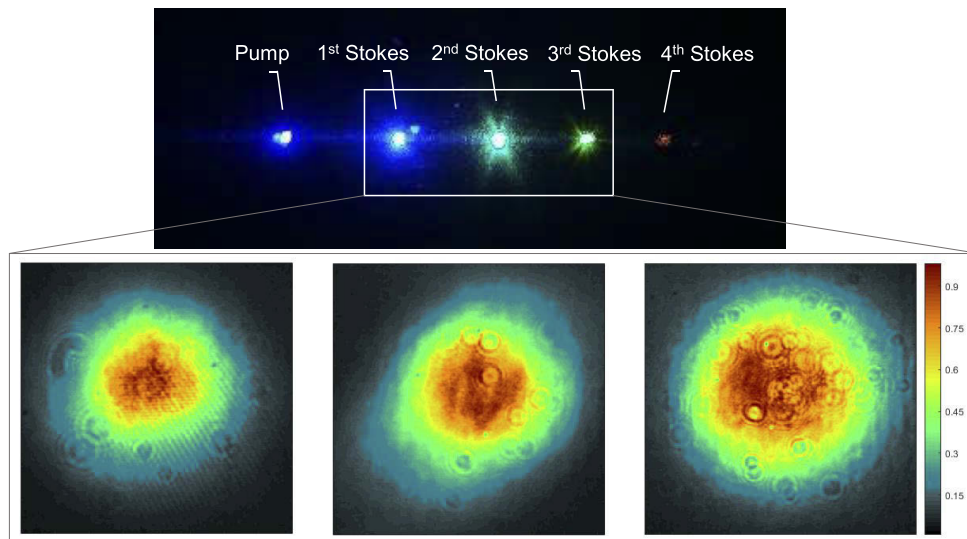
Fig. 5. Measurement of the Stokes near-field beam profiles including the 1st, 2nd and 3rd Stokes orders.

3. Linewidth of Stokes orders

The same LM-007 wavelength meter used to characterize the pump laser was employed to measure the Stokes output linewidth with a resolution of <0.5 GHz. The LM-007 is based on a block of four separated thermally stabilized neon-filled Fizeau interferometers that have different bases (3 μm,

50 μm, 1.5 mm and 40 mm) allowing the spectral characterization of lasers with linewidth ranging from 0.5 - 500 GHz with a resolution up to 40 MHz. For our experiment, although we used the four interferometers simultaneously, only interferometer 3 (with base of 1.5 mm) was well suited to measure the Stokes spectral profiles. The averaged output spectra of the pump, along with the 1st, the 2nd and the 3rd Stokes are depicted in Fig. 6. Here, the Stokes outputs were measured for the same pump power and polarization conditions (900 mW, $\psi_{<100>} = 54°$), optimized for cascading. The results indicate that the output Stokes orders linewidth (at FWHM) match that of the one of the pump laser with a maximum deviation of $< 1.6 \pm 0.2$ GHz. The measured Stokes linewidths were $\Delta\nu_{S1} = 11.5 \pm 0.3$ GHz, $\Delta\nu_{S2} = 9.9 \pm 0.6$ GHz, and $\Delta\nu_{S3} = 12 \pm 0.3$ GHz, for 1st, 2nd and 3rd orders, respectively. The spectral lineshape was close to Lorentzian for both pump and Stokes orders. To our knowledge, this is the first time that the cascaded orders of a narrow-linewidth Raman laser have been spectrally characterized, demonstrating their potential for spectroscopic applications in an extended wavelength range.
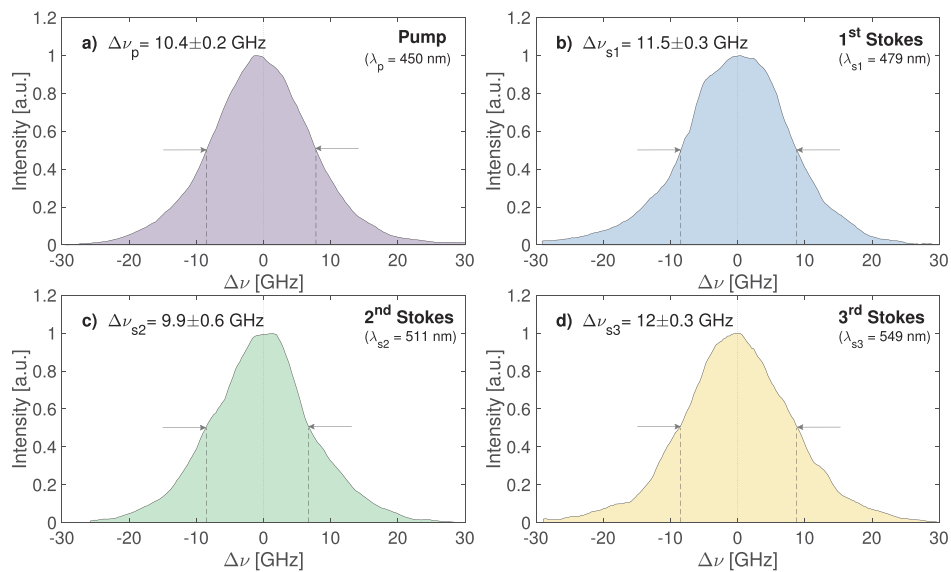
Fig. 6. Measured spectral profiles of (a) pump, (b) 1st Stokes, (c) 2nd Stokes, and (d) 3rd Stokes, using the LM-007 wavelength meter. The spectra were recorded using an integration time of 0.1 s (1000 shots) and a Fizeau interferometer base of 1.5 mm (FSR = 59.9 GHz, instrumental width = 5.26 GHz, resolution < 0.5 GHz).

3.1. Coherent Raman scattering regime

Noticeably, the pump field linewidth was considerably smaller than the spontaneous Stokes noise fields bandwidth (typically > 45 GHz [30]). Since the pump laser linewidth ($\Delta\nu_p = 10.4 \pm 0.2$ GHz) allows fluctuations shorter than 100 ps, and much longer than the dephasing time ($T_2 = 6.2$ ps for diamond [31]), the Raman gain is considered to be in the 'steady-state' regime. The linewidth of the Stokes field is then dictated by the temporal correlation with the pump field. For high intensity pumping fields, the fields are highly correlated, producing a normalised Stokes field that is nearly identical to the fundamental field. Under these conditions, the phonon field is coherently driven to its steady-state value, with the correct phonon phase to coherently scatter the fundamental photons into the Stokes field, achieving the maximum (or monochromatic) Raman gain. This is normally referred as coherent scattering regime.

The cascaded generation of the $(n + 1)^{th}$ Stokes order is rapidly amplified to match the nth Stokes order field. We have observed this phenomena in the temporal profiles, where the 2nd Stokes profile follows precisely the 1st Stokes temporal profile for single-shot traces. In this case, the phonon field that scatters the fundamental field into the 1st Stokes also scatters the nth Stokes order into the $(n + 1)^{th}$ Stokes order, thus maximizing Raman gain through the cascading process. In the frequency domain, the consequence is that all Stokes orders replicate the pump field spectral profile, as shown in Fig. 6.

Even if the pump and 1st Stokes linewidths are nearly identical, the pump has around 25 modes within its linewidth whereas the Stokes has only 3 modes within its linewidth. In general, the number of possible FWM seeding modes generated by M pump modes and N 1st Stokes modes is $M \times N$ modes at the 2nd Stokes wavelength. However, since $\Delta\nu_p = \Delta\nu_{S1} = \Delta\nu_{S2}$, the number of allowed FWM modes within the 2nd Stokes linewidth is reduced to $(M \times N)/2$. FWM can seed in principle ~ 38 modes within the 2nd Stokes linewidth, but only 3 of them are allowed by the resonator effective length. For effective FWM seeding, ~ 3 of the ~ 38 potential FWM seeding modes must overlap spectrally with the allowed longitudinal modes. Statistically, the majority of the output pulses are not FWM seeded. Nonetheless, FWM can still be a dominant force in the early Raman amplification stages. In the frequency domain, the 2nd stokes could be off-mode-centre during the seeding stage due to phase rotation of the mode caused by the seeding, and then come to mode-centre when SRS dominates and the seeding becomes irrelevant.

In order to preserve the linewidth through the cascading process, the pump and Stokes fields must remain highly correlated. However, group velocity dispersion (GVD) causes slippage between the fundamental and Stokes orders envelopes, potentially preventing correlations from building up and even removing existing correlations. Since the cascading process produces light at ever longer wavelengths, dispersion starts to play an important role in the correlations. Even though the GVD may be relatively small between the fundamental and 1st Stokes wavelengths, its cumulative effect after multiple cascaded processes can be detrimental. Here, we define a limit for the dephasing length (z_d) between the fundamental and the nth Stokes order. Dephasing time z_d is defined as the propagation length over which the temporal structure in the fundamental field stays overlapped with a point on the higher-order Stokes envelope. Expressions for z_d have been obtained analytically for top-hat spectral distributions [23]. In our case, for Lorentzian spectra of half width $\Delta\nu_p/2$, the characteristic temporal structure has a duration of $\tau = 1/(\pi\Delta\nu_p)$, where $z_d = 1/(2\pi\Delta\nu_p|\mu|)$. Here $|\mu|$ is the group delay difference per meter between fundamental and Stokes fields.

For excitation at 450 nm and 3rd Stokes generation, the average $|\mu|_{ps_3}$ for the cavity is ≈ 24.9 ps/m , yielding an average $z_d \approx 58$ cm. This length is 6× longer than the total propagated length per cavity lifetime, accordingly GVD is negligible for our case. It is clear from this argument, however, that Raman cavities with higher reflectivity and pumped by broader linewidth fields are more subject to weaker field correlations through the cascading process. In order to maintain correlations, increasing the pump intensity may be sufficient so that the fundamental field can imprint its structure on the Stokes beam faster than that structure becomes misaligned.

Thus, for spectroscopic applications, it is preferred to operate in the coherent scattering regime with high gain and large output coupling, forcing the linewidth of the Stokes orders to be identical to that of the pump. It is worth noting, that the free spectral range (FSR) of the pump laser and the Raman resonator are 300 MHz and 3 GHz respectively. The Stokes field is composed of only 3 longitudinal modes, but still capable of duplicating the pump field temporal profile accurately, even if the mode spacing differs by a factor of ~ 10. The profiles depicted in Fig. 6 are spectral averages over 1000 shots (with randomly positioned longitudinal modes), while individual shots showed wide mode spacing (3 GHz) as expected for the Stokes output.

3.2. Excitation of atomic transitions using the diamond Raman laser

In order to demonstrate that this few-mode Raman laser can be effective for the same spectroscopic application of the pump beam itself, we have performed resonance ionization spectroscopy of calcium, using the atomic transition $4s^2\,^1S_0 \rightarrow 4s4p\,^1P_1^0$ at 422.79 nm. A collimated beam of the 1st Stokes output of the Raman laser was crossing an atomic Ca beam in a perpendicular geometry inside the ionization chamber of a time-of-flight mass-spectrometer. The residual Doppler and saturation broadening of the transition was < 1 GHz, resulting in a dominating contribution of the Raman laser linewidth to the observable width of the spectral resonance.

The tuning of the Stokes wavelength was performed by tuning the wavelength of the Ti:Sapphire laser around 400.25 nm which was calculated from the known values of Ca transition [32] and Raman shift in diamond. The resonantly excited Ca atoms were ionized by the 389.71 nm radiation of another frequency-doubled Ti:Sapphire laser operated synchronously with the Raman laser. The produced Ca^+ yield was measured with a time-of-flight spectrometer, while the wavelength of the Raman laser was measured simultaneously using a *HighFinesse/Ångstrom WS/6* with a resolution better than <0.066 cm^{-1}. The schematic of the atomic transition alongside with the experimental results are shown in Fig. 7. As it can be seen in Fig. 7(b), the resonance had a FWHM of 11.9 ± 0.3 GHz, corresponding to the convolution of the Raman 1st Stokes output with the Ca transition, demonstrating that our Raman laser can be effectively employed for RIS applications. Details regarding this experiment will be given in [33].
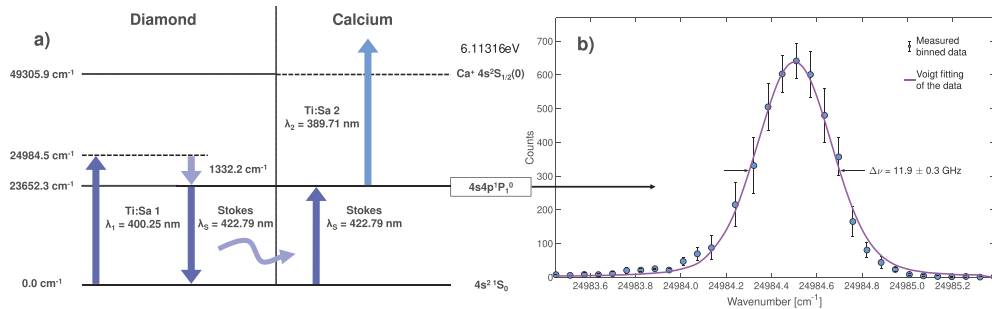
Fig. 7. (a) Diamond Raman shifting and Ca transition $4s^2\,^1S_0 \rightarrow 4s4p\,^1P_1^0$. (b) Scan of the Raman laser pumping wavelength demonstrating a resonance excitation of the Ca atomic transition at 422.79 nm (vacuum).

4. Conclusions and outlook

We demonstrate an all-solid-state continuously tunable laser across the visible range of the spectrum (420 - 600 nm) based on efficient cascading of Raman processes in diamond. We have shown and optimized the design of a Raman converter that simultaneously conserves the pump linewidth while exhibiting a combined conversion efficiency surpassing 60 % from pump to higher Stokes orders. We identified the conditions for maintaining the Stokes linewidth through the cascading process, showing that $\Delta\nu_s = 11 \pm 1$ GHz for all orders. This measurement shows that our Raman laser can be effectively used for spectroscopic applications such as RIS of an atomic vapour.

We also show that optimization of the cascading to higher Stokes orders is achieved by tuning the polarization state of the pump. Additionally, we derived this analytically, showing that maximum cascading is obtained using $\psi_{<100>} = 54.7°$, with all Stokes orders polarized parallel to the <111> axis. In the same way, these analytical expressions are not only capable of predicting the relative gain, but also the output polarization of the orders. We concluded that in order to

preserve the Stokes linewidth through the cascading process it is preferable to operate in the coherent Raman scattering regime, where the field amplitudes of pump and Stokes are highly correlated in the temporal domain. Several factors need to be considered in order to achieve high correlation, in particular: short cavity photon lifetime, high pump intensity, high Raman media gain and low dispersion, and large FSR of the Raman laser cavity.

Furthermore, to the best of our knowledge, this is the first time that a solid-state Raman laser is used for RIS, demonstrated by exciting an electronic transition in calcium at 422.79 nm. The next steps involve the development of narrower and variable linewidth Raman lasers and at a wider range of wavelengths for spectroscopic studies of rare and short-lived isotopes at CERN and other facilities.

Funding

Disclosures

The authors declare no conflicts of interest.

References

1. V. S. Letokhov, *Lasers in Atomic, Molecular, and Nuclear Physics* (World Scientific Publishing Co. Pte. Ltd., 1987).
2. W. Demtröder, *Laser Spectroscopy* (Springer Science & Business Media, 2002).
3. V. S. Letokhov, *Laser Photoionization Spectroscopy* (Academic, 1987).
4. U. Köster, V. Fedoseyev, and V. Mishin, "Resonant laser ionization of radioactive atoms," Spectrochim. Acta, Part B **58**(6), 1047–1068 (2003).
5. V. Fedosseev, K. Chrysalidis, T. Day Goodacre, B. Marsh, S. Rothe, C. Seiffert, and K. Wendt, "Ion beam production and study of radioactive isotopes with the laser ion source at ISOLDE," J. Phys. G: Nucl. Part. Phys. **44**(8), 084006 (2017).
6. S. Rothe, T. D. Goodacre, D. Fedorov, V. Fedosseev, B. Marsh, P. Molkanov, R. Rossel, M. Seliverstov, M. Veinhard, and K. Wendt, "Laser ion beam production at cern-isolde: New features - more possibilities," Nucl. Instrum. Methods Phys. Res., Sect. B **376**, 91–96 (2016).
7. S. Rothe, B. A. Marsh, C. Mattolat, V. N. Fedosseev, and K. Wendt, "A complementary laser system for ISOLDE RILIS," J. Phys.: Conf. Ser. **312**, 052020 (2011).
8. E. Granados, K. Chrysalidis, V. N. Fedosseev, B. A. Marsh, S. G. Wilkins, K. D. A. Wendt, R. P. Mildren, and D. J. Spence, "Continuously tunable diamond raman laser for resonance ionization experiments at cern," in *Laser Congress 2019 (ASSL, LAC, LS&C)*, (Optical Society of America, 2019), p. JW2A.13.
9. H. Pask, "The design and operation of solid-state raman lasers," Prog. Quantum Electron. **27**(1), 3–56 (2003).
10. J. T. Murray, W. L. Austin, and R. C. Powell, "Intracavity raman conversion and raman beam cleanup," Opt. Mater. **11**(4), 353–371 (1999).
11. K. Chrysalidis, V. N. Fedosseev, B. A. Marsh, R. P. Mildren, D. J. Spence, K. D. A. Wendt, S. G. Wilkins, and E. Granados, "Continuously tunable diamond raman laser for resonance laser ionization," Opt. Lett. **44**(16), 3924–3927 (2019).
12. R. Casula, J.-P. Penttinen, M. Guina, A. J. Kemp, and J. E. Hastie, "Cascaded crystalline raman lasers for extended wavelength coverage: continuous-wave, third-stokes operation," Optica **5**(11), 1406–1413 (2018).
13. R. Mildren, M. Convery, H. Pask, J. Piper, and T. Mckay, "Efficient, all-solid-state, raman laser in the yellow, orange and red," Opt. Express **12**(5), 785–790 (2004).
14. R. J. Williams, O. Kitzler, A. McKay, and R. P. Mildren, "Investigating diamond raman lasers at the 100w level using quasi-continuous-wave pumping," Opt. Lett. **39**(14), 4152–4155 (2014).
15. V. G. Savitski, I. Friel, J. E. Hastie, M. D. Dawson, D. Burns, and A. J. Kemp, "Characterization of single-crystal synthetic diamond for multi-watt continuous-wave raman lasers," IEEE J. Quantum Electron. **48**(3), 328–337 (2012).
16. R. J. Williams, O. Kitzler, Z. Bai, S. Sarang, H. Jasbeer, A. McKay, S. Antipov, A. Sabella, O. Lux, D. J. Spence, and R. P. Mildren, "High power diamond raman lasers," IEEE J. Sel. Top. Quantum Electron. **24**(5), 1–14 (2018).
17. J. A. Piper and H. M. Pask, "Crystalline raman lasers," IEEE J. Sel. Top. Quantum Electron. **13**(3), 692–704 (2007).
18. E. Granados, D. J. Spence, and R. P. Mildren, "Deep ultraviolet diamond raman laser," Opt. Express **19**(11), 10857–10863 (2011).
19. A. Sabella, J. A. Piper, and R. P. Mildren, "Diamond raman laser with continuously tunable output from 3.38 to 3.80 μm," Opt. Lett. **39**(13), 4037–4040 (2014).
20. P. Latawiec, V. Venkataraman, M. J. Burek, B. J. M. Hausmann, I. Bulu, and M. Lončar, "On-chip diamond raman laser," Optica **2**(11), 924–928 (2015).

21. S. Reilly, V. G. Savitski, H. Liu, E. Gu, M. D. Dawson, and A. J. Kemp, "Monolithic diamond raman laser," Opt. Lett. **40**(6), 930–933 (2015).
22. O. Lux, S. Sarang, R. J. Williams, A. McKay, and R. P. Mildren, "Single longitudinal mode diamond raman laser in the eye-safe spectral region for water vapor detection," Opt. Express **24**(24), 27812–27820 (2016).
23. D. J. Spence, "Spectral effects of stimulated raman scattering in crystals," Prog. Quantum Electron. **51**, 1–45 (2017).
24. G. Hernandez, *Cambridge Studies in Modern Optics 3: Fabry - Perot Interferometers* (Cambridge University, 1986).
25. A. Sabella, J. A. Piper, and R. P. Mildren, "1240 nm diamond raman laser operating near the quantum limit," Opt. Lett. **35**(23), 3874–3876 (2010).
26. R. P. Mildren, J. E. Butler, and J. R. Rabeau, "Cvd-diamond external cavity raman laser at 573 nm," Opt. Express **16**(23), 18950–18955 (2008).
27. R. P. Mildren, D. W. Coutts, and D. J. Spence, "All-solid-state parametric raman anti-stokes laser at 508 nm," Opt. Express **17**(2), 810–819 (2009).
28. T. T. Basiev, S. N. Smetanin, A. S. Shurygin, and A. V. Fedin, "Parametric coupling of frequency components at stimulated raman scattering in solids," Phys.-Usp. **53**(6), 611–617 (2010).
29. A. McKay, A. Sabella, and R. P. Mildren, "Polarization conversion in cubic Raman crystals," Sci. Rep. **7**(1), 41702 (2017).
30. M. S. Liu, L. A. Bursill, S. Prawer, and R. Beserman, "Temperature dependence of the first-order raman phonon line of diamond," Phys. Rev. B **61**(5), 3391–3395 (2000).
31. K. Lee, B. J. Sussman, J. Nunn, V. Lorenz, K. Reim, D. Jaksch, I. Walmsley, P. Spizzirri, and S. Prawer, "Comparing phonon dephasing lifetimes in diamond using transient coherent ultrafast phonon spectroscopy," Diamond Relat. Mater. **19**(10), 1289–1295 (2010).
32. A. Kramida, Yu. Ralchenko, J. Reader, and and NIST ASD Team, NIST Atomic Spectra Database (ver. 5.7.1), [Online]. Available: https://physics.nist.gov/asd [2019, November 28]. National Institute of Standards and Technology, Gaithersburg, MD. (2019).
33. K. Chrysalidis, D. T. Echarri, V. N. Fedosseev, B. A. Marsh, S. M. Olaizola, S. G. Wilkins, and E. Granados. Are preparing a manuscript to be called "First application of a diamond Raman laser for resonance ionization spectroscopy".